Variational Mode Decomposition

Konstantin Dragomiretskiy and Dominique Zosso, *Member, IEEE*

Abstract—During the late 1990s, Huang introduced the algorithm called Empirical Mode Decomposition, which is widely used today to recursively decompose a signal into different modes of unknown but separate spectral bands. EMD is known for limitations like sensitivity to noise and sampling. These limitations could only partially be addressed by more mathematical attempts to this decomposition problem, like synchrosqueezing, empirical wavelets or recursive variational decomposition. Here, we propose an entirely non-recursive variational mode decomposition model, where the modes are extracted concurrently. The model looks for an ensemble of modes and their respective center frequencies, such that the modes collectively reproduce the input signal, while each being smooth after demodulation into baseband. In Fourier domain, this corresponds to a narrow-band prior. We show important relations to Wiener filter denoising. Indeed, the proposed method is a generalization of the classic Wiener filter into multiple, adaptive bands. Our model provides a solution to the decomposition problem that is theoretically well founded and still easy to understand. The variational model is efficiently optimized using an alternating direction method of multipliers approach. Preliminary results show attractive performance with respect to existing mode decomposition models. In particular, our proposed model is much more robust to sampling and noise. Finally, we show promising practical decomposition results on a series of artificial and real data.

Index Terms—AM-FM, augmented Lagrangian, Fourier transform, Hilbert transform, mode decomposition, spectral decomposition, variational problem, Wiener filter.

I. INTRODUCTION

EMPIRICAL MODE decompositon (EMD) proposed by Huang *et al.* [1] is an algorithmic method to detect and decompose a signal into principal "modes". This algorithm recursively detects local minima/maxima in a signal, estimates lower/upper envelopes by interpolation of these extrema, removes the average of the envelopes as "low-pass" centerline, thus isolating the high-frequency oscillations as "mode" of a signal, and continues recursively on the remaining "low-pass" centerline. In some cases, this sifting algorithm does indeed decompose a signal into principal modes, however the resulting decomposi-

tion is highly dependent on methods of extremal point finding, interpolation of extremal points into carrier envelopes, and the stopping criteria imposed. The lack of mathematical theory and the aforementioned degrees of freedom reducing the algorithm's robustness all leave room for theoretical development and improvement on the robustness of the decomposition [2]–[5]. In some experiments it has been shown that EMD shares important similarities with wavelets and (adaptive) filter banks [6].

Despite the limited mathematical understanding and some obvious shortcomings, the EMD method has had significant impact and is widely used in a broad variety of time-frequency analysis applications. These involve signal decomposition in audio engineering [7], climate analysis [8], and various flux, respiratory, and neuromuscular signals found in medicine and biology [9]–[12], to name just a few examples.

A. What is a Mode?

In the original EMD description, a mode is defined as a signal whose number of local extrema and zero-crossings differ at most by one [1]. In most later related works, the definition is slightly changed into so-called *Intrinsic Mode Functions* (IMF), based on modulation criteria:

*Definition 1: (***Intrinsic Mode Function***):* Intrinsic Mode Functions are amplitude-modulated-frequency-modulated (AM-FM) signals, written as:

$$u_k(t) = A_k(t) \cos\left(\phi_k(t)\right), \qquad (1)$$

where the phase $\phi_k(t)$ is a non-decreasing function, $\phi_k'(t) \geq 0$, the envelope is non-negative $A_k(t) \geq 0$, and, very importantly, both the envelope $A_k(t)$ and the instantaneous frequency $\omega_k(t) := \phi_k'(t)$ vary much slower than the phase $\phi_k(t)$ [13], [14].

In other words, on a sufficiently long interval $[t-\delta, t+\delta], \delta \approx 2\pi/\phi_k'(t)$, the mode $u_k(t)$ can be considered to be a pure harmonic signal with amplitude $A_k(t)$ and instantaneous frequency $\phi_k'(t)$ [13]. Note that the newer definition of signal components is slightly more restrictive than the original one: while all signals adhering to the above IMF definition satisfy the original EMD mode properties, the converse is not necessarily true [13]. The immediate consequence of the newer IMF definition, however, is limited bandwidth, as we show in the next paragraphs, and which is the central assumption that allows mode separation in the proposed variational mode decomposition model. Our restricted class of admissible mode functions is also motivated by analysis in [3], for they are well-behaved with respect to time-frequency analysis of extracted modes, as routinely performed in the Hilbert-Huang-Transform [1]. In contrast, the original IMF definition also admits non-C^1 and discontinuous signals like the sawtooth, for which the estimated instantaneous frequency is not physically meaningful, see Fig. 1.
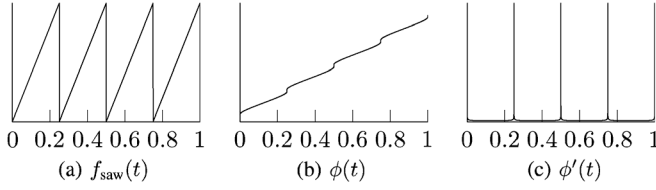
Fig. 1. Sawtooth signal and its phase/frequency. (a) The original signal. (b) The estimated phase after Hilbert transform. The phase exhibits jumps at the discontinuous saw-peaks. (c) The instantaneous frequency is obtained as the time-derivative of the phase. At the discontinuous saw-peaks, this is clearly meaningless. Such a signal is an admissible mode according to the original IMF definition based on zero-crossings and local extrema [1], but not part of the newer definition based on amplitude- and frequency-modulated signals (1) which is also used here [13].

Indeed, if ω_k is the mean frequency of a mode, then its practical bandwidth increases both with the maximum deviation Δf of the instantaneous frequency from its center (carrier frequency, f_c), and with the rate of this excursion, f_{FM}, according to **Carson's rule**[1] [15]:

$$BW_{\text{FM}} = 2(\Delta f + f_{\text{FM}}). \qquad (2)$$

In addition to this, the bandwidth of the envelope $A_k(t)$ modulating the amplitude of the FM signal, itself given by its highest frequency f_{AM}, broadens the spectrum even further:

*Definition 2: (***Total Practical IMF Bandwidth***):* We estimate the total practical bandwidth of an IMF as

$$BW_{\text{AM−FM}} = 2(\Delta f + f_{\text{FM}} + f_{\text{AM}}). \qquad (3)$$

Depending on the actual IMF, either of these terms may be dominant. An illustration of four typical cases is provided in Fig. 2, where the last example is rather extreme in terms of required bandwidth (for illustrational purposes).

B. Recent Work

To address the sensitivity of the original EMD algorithm with respect to noise and sampling, more robust versions have since been proposed [16], [17]. There, in essence, the extraction of local extrema and their interpolation for envelope forming is substituted by more robust constraint optimization techniques. The global recursive sifting structure of EMD is maintained, however.

Other authors create a partially variational approach to EMD where the signal is explicitly modeled as an IMF [18]. This method still relies on interpolation, selection of a Fourier low-pass filter, and sifting of high-frequency components. Here, the candidate modes are extracted variationally. The signal is recursively decomposed into an IMF with TV3-smooth envelope (3rd-order total variation), and a TV3-smooth residual. The resulting algorithm is very similar to EMD in structure, but somewhat more robust to noise.

A slightly more variational, but still recursive decomposition scheme has been proposed in [19], for the analysis of time-varying vibration. Here, the dominant vibration is extracted
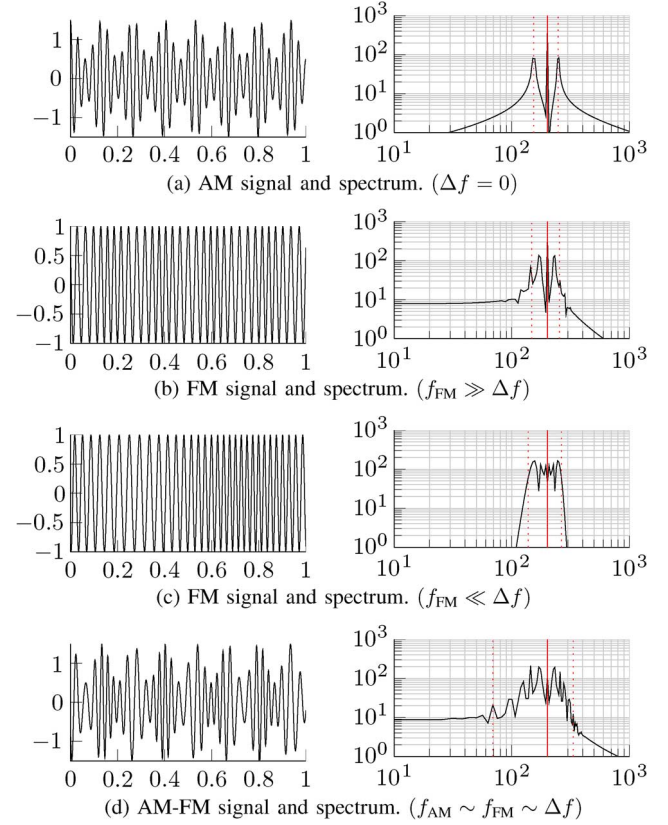
Fig. 2. AM-FM signals with limited bandwidth. Here, we use a signal $f(t) = (1 + 0.5 \cos(2\pi f_{\text{AM}}t))\cdot\cos(2\pi f_c t + \Delta f/f_{\text{FM}}\cos(2\pi f_{\text{FM}}t))$. (a) Pure AM signal. (b) Pure FM signal with little but rapid frequency deviations. (c) Pure FM signal with slow but important frequency oscillations. (d) Combined AM-FM signal. The solid vertical line in the spectrum shows the carrier frequency f_c, the dotted lines correspond to the estimated band limits at $f_c \pm BW/2$, based on (3).

by estimating its instantaneous frequency as average frequency after the Hilbert transform. Again, this process is repeated recursively on the residual signal.

A third class of methods makes use of wavelets. An approach based on selecting appropriate wavelet scales, dubbed *synchrosqueezing*, was proposed by Daubechies *et al.* [13], [20]. They remove unimportant wavelet coefficients (both in time and scale) by thresholding of the respective signal energy in that portion. Conversely, locally relevant wavelets are selected as local maxima of the continuous wavelet transform, that are shown to be tuned with the local signals, and from which the current instantaneous frequency of each mode can be recovered.

Other recent work pursuing the same goal is the Empirical Wavelet Transform (EWT) to explicitly build an adaptive wavelet basis to decompose a given signal into adaptive sub-bands [14]. This model relies on robust preprocessing for peak detection, then performs spectrum segmentation based on detected maxima, and constructs a corresponding wavelet filter bank. The filter bank includes flexibility for some mollification (spectral overlap), but explicit construction of frequency bands still appears slightly strict.

Finally, a related decomposition into different wavelet bands was suggested by [21]. The author introduces two complementary wavelet bases with different Q-factor. This allows discrim-

---

[1]The theoretical spectral support of a frequency modulated signal is infinite; However, for practical purposes, Carson's rule provides bounds containing 98% of the signal's power, which should be good enough in this context.

inating between sustained oscillations (high-resonance components), and non-oscillatory, short-term transients. Indeed, the high-resonance components can sparsely be represented in a high-Q wavelet basis, while transients will be synthesized by low-Q wavelets.

C. Proposed Method

In this paper, we propose a new, fully intrinsic and adaptive, variational method, the minimization of which leads to a decomposition of a signal into its principal modes. Indeed, the current decomposition models are mostly limited by 1) their algorithmic ad-hoc nature lacking mathematical theory (EMD), 2) the recursive sifting in most methods, which does not allow for backward error correction, 3) the inability to properly cope with noise, 4) the hard band-limits of wavelet approaches, and 5) the requirement of predefining filter bank boundaries in EWT. In contrast, we propose a variational model that determines the relevant bands adaptively, and estimates the corresponding modes concurrently, thus properly balancing errors between them. Motivated by the narrow-band properties corresponding to the current common IMF definition, we look for an ensemble of modes that reconstruct the given input signal optimally (either exactly, or in a least-squares sense), while each being band-limited about a center frequency estimated on-line. Here, our variational model specifically can address the presence of noise in the input signal. Indeed, the tight relations to the Wiener filter actually suggest that our approach has some optimality in dealing with noise. The variational model assesses the bandwidth of the modes as H^1-norm, after shifting the Hilbert-complemented, analytic signal down into baseband by complex harmonic mixing. The resulting optimization scheme is very simple and fast: each mode is iteratively updated directly in Fourier domain, as the narrow-band Wiener filter corresponding to the current estimate of the mode's center-frequency being applied to the signal estimation residual of all other modes; then the center frequency is re-estimated as the center-of-gravity of the mode's power spectrum. Our quantitative results on tone detection and separation show excellent performance irrespective of harmonic frequencies, in particular when compared to the apparent limits of EMD in this respect. Further, qualitative results on synthetic and real test signals are convincing, also regarding robustness to signal noise.

The rest of this paper is organized as follows: Section II introduces the notions of the Wiener filter, the Hilbert transform, and the analytic signal. Also, we briefly review the concept of frequency shifting through harmonic mixing. These concepts are the very building blocks of our variational mode decomposition model. Although signal processing scholars can be expected to be familiar with these concepts, we include this short refresher to keep the manuscript largely self-contained and accessible to readers of different provenience. Section III presents and explains our variational model in detail, our algorithm to minimize it, and finer technicalities on optimization, boundaries and periodicity. Section IV contains our experiments and results, namely some simple quantitative performance evaluations, and

comparisons to EMD, and various synthetic multi-mode signals and our method's decomposition of them. Specifically, tone detection and separation, as well as noise robustness will be analyzed and compared to that of EMD. Additionally, real signals will be considered. Section V concludes on our proposed variational mode decomposition method, summarizes again the main assumptions and limitations, and includes some future directions and expected improvements.

II. TOOLS FROM SIGNAL PROCESSING

In this section we briefly review a few concepts and tools from signal processing that will constitute the building blocks of our variational mode decomposition model. First, we present a classical case of Wiener filtering for denoising. Next, we describe the Hilbert transform and its use in the construction of a single-side band analytic signal. Finally, we show how multiplication with pure complex harmonics is used to shift the frequencies in a signal.

A. Wiener Filtering

Let us start with a simple denoising problem. Consider the observed signal $f_0(t)$, a copy of the original signal $f(t)$ affected by additive zero-mean Gaussian noise:

$$f_0 = f + \eta \tag{4}$$

Recovering the unknown signal f is a typical ill-posed inverse problem [22], [23], classically addressed using Tikhonov regularization [24], [25]:

$$\min_f \left\{ \|f - f_0\|_2^2 + \alpha \|\partial_t f\|_2^2 \right\}, \tag{5}$$

of which the Euler-Lagrange equations are easily obtained and typically solved in Fourier domain:

$$\hat{f}(\omega) = \frac{\hat{f}_0}{1 + \alpha \omega^2}, \tag{6}$$

where $\hat{f}(\omega) := \mathcal{F}\{f(\cdot)\}(\omega) := 1/\sqrt{2\pi} \int_{\mathbb{R}} f(t)e^{-j\omega t}dt$, with $j^2 = -1$, is the Fourier transform of the signal $f(t)$. Clearly, the recovered signal f is a low-pass narrow-band selection of the input signal f_0 around $\omega = 0$. Indeed, the solution corresponds to convolution with a Wiener filter, where α represents the variance of the white noise, and the signal has a lowpass $1/\omega^2$ power spectrum prior [26], [27].

B. Hilbert Transform and Analytic Signal

Here, we cite the definition of the Hilbert transform given in [28]:

*Definition 3: (**Hilbert Transform**):* The 1-D Hilbert transform is the linear, shift-invariant operator $\mathcal{H}$ that maps all 1-D cosine functions into their corresponding sine functions. It is an all-pass filter that is characterized by the transfer function $\hat{h}(\omega) = -j\,\mathrm{sgn}(\omega) = -j\omega/|\omega|$.

Thus, the Hilbert transform is a multiplier operator in the spectral domain. The corresponding impulse response is

$h(t) = 1/(\pi t)$. Because convolution with $h(t)$ is not integrable, the Hilbert transform $\mathcal{H}f(t)$ of a signal $f(t)$ is obtained as the Cauchy principal value (denoted p.v.) of the convolution integral:

$$\mathcal{H}f(t) = \frac{1}{\pi}\text{p.v.} \int_{\mathbb{R}} \frac{f(v)}{t-v}dv. \quad (7)$$

For further properties and analysis of the Hilbert transform, we refer e.g. to [29].

The most prominent use of the Hilbert transform is in the construction of an analytic signal from a purely real signal, as proposed by Gabor [30].

*Definition 4: (**Analytic Signal**):* Let $f(t)$ be a purely real signal. The complex-valued analytic signal is now defined as:

$$f_A(t) = f(t) + j\mathcal{H}f(t) = A(t)e^{j\phi(t)}. \quad (8)$$

This analytic signal has the following important properties. The complex exponential term $e^{j\phi(t)}$ is a phasor describing the rotation of the complex signal in time, $\phi(t)$ being the phase, while the amplitude is governed by the real envelope $A(t)$. This representation is particularly useful in the analysis of time-varying amplitude and instantaneous frequency, defined as $\omega(t) = d\phi(t)/dt$. In particular for IMF signals of the form (1), where the amplitude A_k changes slowly enough, Bedrosian's theorem applies [31], and the analytic signal directly inherits the same amplitude function:

$$u_{k,A}(t) = A_k(t)\left(\cos\left(\phi(t)\right) + j\sin\left(\phi(t)\right)\right)$$
$$= A_k(t)e^{j\phi(t)}. \quad (9)$$

The second property is the unilateral spectrum of the analytic signal, consisting only of non-negative frequencies. Finally, we note that from such an analytic signal, the original (real) signal is easily retrieved as the real part:

$$f(t) = \Re\left\{f_A(t)\right\}. \quad (10)$$

C. Frequency Mixing and Heterodyne Demodulation

The last concept that we wish to recall before introducing the proposed variational mode decomposition, is the principle of frequency mixing. Mixing is the process of combining two signals non-linearly, thus introducing cross-frequency terms in the output. The simplest mixer is multiplication. Multiplying two real signals with frequencies ω_1 and ω_2, respectively, creates mixed frequencies in the output at $\omega_1 - \omega_2$ and $\omega_1 + \omega_2$, which is easily illustrated by the following trigonometric identity:

$$2\cos(\omega_1 t)\cos(\omega_2 t) = \cos\left((\omega_1 + \omega_2)t\right) + \cos\left((\omega_1 - \omega_2)t\right). \quad (11)$$

Here we mix the two respective analytic signals:

$$e^{j\omega_1 t}e^{j\omega_2 t} = e^{j(\omega_1 + \omega_2)t}, \quad (12)$$

and thus, the mixed signal is automatically "mono-tone" (constituted of a single frequency only). In Fourier terms, this is well known as the following transform pair:

$$f_A(t)e^{-j\omega_0 t} \xleftrightarrow{\mathcal{F}} \hat{f}_A(\omega) * \delta(\omega + \omega_0) = \hat{f}_A(\omega + \omega_0), \quad (13)$$

where δ is the Dirac distribution and $*$ denotes convolution. Thus, multiplying an analytic signal with a pure exponential results in simple frequency shifting.

III. VARIATIONAL MODE DECOMPOSITION

In this section we introduce our proposed model for variational mode decomposition, essentially based on the three concepts outlined in the previous section.

The goal of VMD is to decompose a real valued input signal f into a discrete number of sub-signals (modes), u_k, that have specific sparsity properties while reproducing the input.[2] Here, the sparsity prior of each mode is chosen to be its bandwidth in spectral domain. In other words, we assume each mode k to be mostly compact around a center pulsation ω_k, which is to be determined along with the decomposition.

In order to assess the bandwidth of a mode, we propose the following scheme: 1) for each mode u_k, compute the associated analytic signal by means of the Hilbert transform in order to obtain a unilateral frequency spectrum. 2) for each mode, shift the mode's frequency spectrum to "baseband", by mixing with an exponential tuned to the respective estimated center frequency. 3) The bandwidth is now estimated through the H^1 Gaussian smoothness of the demodulated signal, i.e. the squared L^2-norm of the gradient. The resulting constrained variational problem is the following:

$$\min_{\{u_k\},\{\omega_k\}} \left\{ \sum_k \left\| \partial_t \left[\left(\delta(t) + \frac{j}{\pi t} \right) * u_k(t) \right] e^{-j\omega_k t} \right\|_2^2 \right\}$$
$$\text{s.t.} \quad \sum_k u_k = f \quad (14)$$

where $\{u_k\} := \{u_1, \ldots, u_K\}$ and $\{\omega_k\} := \{\omega_1, \ldots, \omega_K\}$ are shorthand notations for the set of all modes and their center frequencies, respectively. Equally, $\sum_k := \sum_{k=1}^{K}$ is understood as the summation over all modes.

The reconstruction constraint can be addressed in different ways. Here, we suggest making use of both a quadratic penalty term and Lagrangian multipliers, λ, in order to render the problem unconstrained. The quadratic penalty is a classic way to encourage reconstruction fidelity, typically in the presence of additive i.i.d. Gaussian noise. The weight of the penalty term is derived from such a Bayesian prior to be inversely proportional to the noise level in the data. Conversely, in a noisefree setting, the weight needs to be infinitely big in order to enforce strict data fidelity, rendering the system ill-conditioned in the process. On the other hand, Lagrangian multipliers are a common way of enforcing constraints strictly. The combination of the two terms

---

[2]For the sake of completeness, we require that both signal and modes are integrable, and square integrable upto second derivatives: $f, u_k \in L^1 \cap W^{2,2}$. We call this functional space X for further reference. This ensures that later integrals are finite, and that Fourier isometry applies. In practice, we will deal with discrete signals and in our implementations the solutions are tacitly discretized.

thus benefits both from the nice convergence properties of the quadratic penalty at finite weight, and the strict enforcement of the constraint by the Lagrangian multiplier. Therefore, we introduce the augmented Lagrangian $\mathcal{L}$ as follows [32], [33]:

$$
\mathcal{L}\left(\{u_k\},\{\omega_k\},\lambda\right) := \alpha \sum_k \left\| \partial_t \left[\left(\delta(t) + \frac{j}{\pi t} \right) * u_k(t) \right] e^{-j\omega_k t} \right\|_2^2
$$

$$
+ \left\| f(t) - \sum_k u_k(t) \right\|_2^2 + \left\langle \lambda(t), f(t) - \sum_k u_k(t) \right\rangle. \quad (15)
$$

The solution to the original minimization problem (14) is now found as the saddle point of the augmented Lagrangian $\mathcal{L}$ in a sequence of iterative sub-optimizations called alternate direction method of multipliers (ADMM) [34]–[36], see algorithm 1. In the next paragraphs, we will then detail how the respective sub-problems can be solved.

Algorithm 1: ADMM optimization concept for VMD

Initialize $\{u_k^1\}, \{\omega_k^1\}, \lambda^1, n \leftarrow 0$
repeat

  $n \leftarrow n + 1$

  for $k = 1 : K$ **do**

    Update u_k:

$$
u_k^{n+1} \leftarrow \underset{u_k}{\arg\min}\, \mathcal{L}\left(\{u_{i<k}^{n+1}\}, \{u_{i\geq k}^n\}, \{\omega_i^n\}, \lambda^n\right) \quad (16)
$$

  end for

  for $k = 1 : K$ **do**

    Update ω_k:

$$
\omega_k^{n+1} \leftarrow \underset{\omega_k}{\arg\min}\, \mathcal{L}\left(\{u_i^{n+1}\}, \{\omega_{i<k}^{n+1}\}, \{\omega_{i\geq k}^n\}, \lambda^n\right) \quad (17)
$$

  end for

  Dual ascent:

$$
\lambda^{n+1} \leftarrow \lambda^n + \tau \left(f - \sum_k u_k^{n+1} \right) \quad (18)
$$

until convergence: $\sum_k \|u_k^{n+1} - u_k^n\|_2^2 / \|u_k^n\|_2^2 < \epsilon$.

A. Minimization w.r.t. u_k

To update the modes u_k, we first rewrite the subproblem (16) as the following equivalent minimization problem:

$$
u_k^{n+1} = \underset{u_k \in X}{\arg\min} \left\{ \alpha \left\| \partial_t \left[\left(\delta(t) + \frac{j}{\pi t} \right) * u_k(t) \right] e^{-j\omega_k t} \right\|_2^2 \right.
$$

$$
\left. + \left\| f(t) - \sum_i u_i(t) + \frac{\lambda(t)}{2} \right\|_2^2 \right\}, \quad (19)
$$

where for simplicity we omit the $\cdot^n$ and $\cdot^{n+1}$ for the fixed directions ω_k and $u_{i\neq k}$, respectively, but each is implicitly understood as the most recent available update. Now, making use of the Parseval/Plancherel Fourier isometry under the L^2 norm, this problem can be solved in spectral domain:

$$
\hat{u}_k^{n+1} = \underset{\hat{u}_k, u_k \in X}{\arg\min} \left\{ \alpha \left\| j\omega \left[(1 + \mathrm{sgn}(\omega + \omega_k))\, \hat{u}_k(\omega + \omega_k) \right] \right\|_2^2 \right.
$$

$$
\left. + \left\| \hat{f}(\omega) - \sum_i \hat{u}_i(\omega) + \frac{\hat{\lambda}(\omega)}{2} \right\|_2^2 \right\}. \quad (20)
$$

We now perform a change of variables $\omega \leftarrow \omega - \omega_k$ in the first term:

$$
\hat{u}_k^{n+1} = \underset{\hat{u}_k, u_k \in X}{\arg\min} \left\{ \alpha \left\| j(\omega - \omega_k) \left[(1 + \mathrm{sgn}(\omega))\, \hat{u}_k(\omega) \right] \right\|_2^2 \right.
$$

$$
\left. + \left\| \hat{f}(\omega) - \sum_i \hat{u}_i(\omega) + \frac{\hat{\lambda}(\omega)}{2} \right\|_2^2 \right\}. \quad (21)
$$

Exploiting the Hermitian symmetry of the real signals in the reconstruction fidelity term, we can write both terms as half-space integrals over the non-negative frequencies:

$$
\hat{u}_k^{n+1} = \underset{\hat{u}_k, u_k \in X}{\arg\min} \left\{ \int_0^\infty 4\alpha(\omega - \omega_k)^2 \left| \hat{u}_k(\omega) \right|^2 \right.
$$

$$
\left. + 2 \left| \hat{f}(\omega) - \sum_i \hat{u}_i(\omega) + \frac{\hat{\lambda}(\omega)}{2} \right|^2 d\omega \right\}. \quad (22)
$$

The solution of this quadratic optimization problem is readily found by letting the first variation vanish for the positive frequencies:

$$
\hat{u}_k^{n+1}(\omega) = \frac{\hat{f}(\omega) - \sum_{i\neq k} \hat{u}_i(\omega) + \frac{\hat{\lambda}(\omega)}{2}}{1 + 2\alpha(\omega - \omega_k)^2}, \quad (23)
$$

which is clearly identified as a Wiener filtering of the current residual, with signal prior $1/(\omega - \omega_k)^2$. The full spectrum of the real mode is then simply obtained by Hermitian symmetric completion. Conversely, the mode in time domain is obtained as the real part of the inverse Fourier transform of this filtered analytic signal.

B. Minimization w.r.t. ω_k

The center frequencies ω_k do not appear in the reconstruction fidelity term, but only in the bandwidth prior. The relevant problem thus reads:

$$
\omega_k^{n+1} = \underset{\omega_k}{\arg\min} \left\{ \left\| \partial_t \left[\left(\delta(t) + \frac{j}{\pi t} \right) * u_k(t) \right] e^{-j\omega_k t} \right\|_2^2 \right\}. \quad (24)
$$

As before, the optimization can take place in Fourier domain, and we end up optimizing:

$$
\omega_k^{n+1} = \underset{\omega_k}{\arg\min} \left\{ \int_0^\infty (\omega - \omega_k)^2 \left| \hat{u}_k(\omega) \right|^2 d\omega \right\}, \quad (25)
$$

This quadratic problem is easily solved as:

$$\omega_k^{n+1} = \frac{\int_0^\infty \omega \, |\hat{u}_k(\omega)|^2 \, d\omega}{\int_0^\infty |\hat{u}_k(\omega)|^2 \, d\omega}, \tag{26}$$

which puts the new ω_k at the center of gravity of the corresponding mode's power spectrum. This mean carrier frequency is the frequency of a least squares linear regression to the instantaneous phase observed in the mode.

Plugging the solutions of the sub-optimizations into the ADMM algorithm 1, and directly optimizing in Fourier domain where appropriate, we get the complete algorithm for variational mode decomposition, summarized in algorithm 2.

Algorithm 2: Complete optimization of VMD

Initialize $\{\hat{u}_k^1\}$, $\{\omega_k^1\}$, $\hat{\lambda}^1$, $n \leftarrow 0$

repeat

    $n \leftarrow n+1$

    for $k = 1 : K$ **do**

        Update $\hat{u}_k$ for all $\omega \geq 0$:

$$\hat{u}_k^{n+1}(\omega) \leftarrow \frac{\hat{f}(\omega) - \sum_{i<k} \hat{u}_i^{n+1}(\omega) - \sum_{i>k} \hat{u}_i^n(\omega) + \frac{\hat{\lambda}^n(\omega)}{2}}{1 + 2\alpha \left(\omega - \omega_k^n\right)^2} \tag{27}$$

        Update ω_k:

$$\omega_k^{n+1} \leftarrow \frac{\int_0^\infty \omega \left|\hat{u}_k^{n+1}(\omega)\right|^2 d\omega}{\int_0^\infty \left|\hat{u}_k^{n+1}(\omega)\right|^2 d\omega} \tag{28}$$

    end for

    Dual ascent for all $\omega \geq 0$:

$$\hat{\lambda}^{n+1}(\omega) \leftarrow \hat{\lambda}^n(\omega) + \tau \left(\hat{f}(\omega) - \sum_k \hat{u}_k^{n+1}(\omega) \right) \tag{29}$$

until convergence: $\sum_k \|\hat{u}_k^{n+1} - \hat{u}_k^n\|_2^2 / \|\hat{u}_k^n\|_2^2 < \epsilon$.

C. Exact Reconstruction Versus Denoising

Here, the role of the Lagrangian multiplier is to enforce the constraint, while the quadratic penalty improves convergence. If exact reconstruction is not the goal, in particular in the presence of (strong) noise that should not be included in the decomposition, using the quadratic penalty only while dropping the Lagrangian multiplier would be the appropriate choice. Indeed, the quadratic penalty on its own represents the least-squares data fidelity prior associated with additive Gaussian noise. The Lagrangian multiplier is effectively shut-off by keeping its value at 0, most easily by simply choosing its update parameter $\tau = 0$.

D. On Boundaries and Periodicity

Up until now, the signals f and the modes u_k have been considered continuous over the whole axis $t \in \mathbb{R}$. However, in signal processing we are much more likely to be working with signals that are both finite in time and resolution. Let us say we restrict the time window to $t \in [0, 1]$. The results presented so far equally hold for discrete, finite time signals, where simply the continuous Fourier transform is replaced by its discrete counterpart. The only problems arise at the boundaries of the signal.

Indeed, when considering short-time signals, the implicit assumption here is that the signal considered is just a one-period extract of an infinitely long, periodic signal. Consequently, the spectrum of a seemingly simple "general trend"-function on a short interval, say $f : [0, 1] \mapsto \mathbb{R}: f(t) = t$, contains an important amount of high-frequency harmonics, since we are effectively looking at the spectrum of the periodic sawtooth function. Conversely in time domain, we realize that at the endpoints of the domain, the periodized function is discontinuous, thus severely affecting the H^1 smoothing term.

There are several possible remedies to this. Ideally, one should exclude the boundaries of the domain in the evaluation of the smoothness, i.e. restrict its evaluation to the open interval (0,1). However, this clearly breaks the Parseval/Plancherel Fourier isometry and the whole beauty of the spectral solution is lost.

Here, the boundary issues can most easily be remedied by simple mirror extension of the signal by half its length on each side, effectively corresponding to Neumann boundary conditions, namely vanishing derivatives at the time domain boundaries. We will briefly discuss an alternative for short-time analysis of non-stationary signals in the last section of this paper.

IV. EXPERIMENTS AND RESULTS

In this section, we apply the proposed VMD algorithm to a series of test signals in order to assess the validity of our approach. First, we focus on a few problems that have been successfully employed for highlighting the strengths and shortcomings of EMD, namely tones versus sampling, and tones separation [2]. Then we briefly investigate noise robustness of VMD, sensitivity to initialization and over- and underbinning (choice of K). Finally, we shift our attention to more complex signals, which have already been used for evaluation in [18] and [14].

A. Tones and Sampling

When the input signal $f = f_\nu(t) = \cos(2\pi\nu t)$ is composed of a pure harmonic, then the mode decomposition is expected to output exactly this harmonic. As reported in [2], [5], this does not happen to be the case with EMD, since the local extrema can suffer from important jittering with increasing frequency. In [2], the relative error

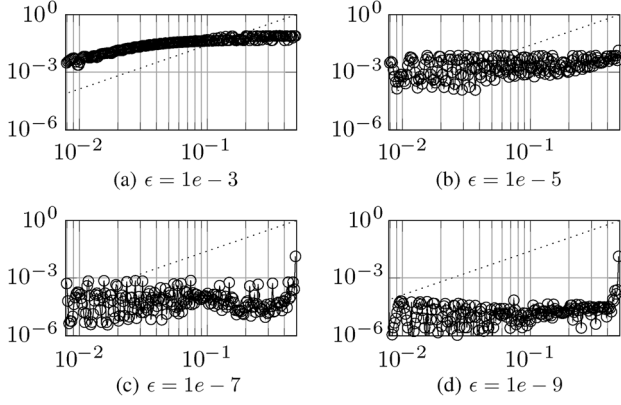$$e(\nu) = \frac{\|f_\nu(t) - u_1(t)\|_2}{\|f_\nu(t)\|_2} \tag{30}$$

Fig. 3. Mode decomposition of a pure harmonic. (a)–(d) Relative error for a range of 257 frequencies, for different convergence tolerance levels ϵ. The relative error does not correlate with the tone frequency. Further, reconstruction error can be controlled by decreasing the stopping criterion's convergence tolerance, except for frequencies very close to the Nyquist frequency. In contrast, EMD's relative tone reconstruction error is bounded by a quadratic increase with frequency (dotted line) [2].

was introduced, and a quadratic increase with frequency of an upper bound to this relative error was reported for EMD. Further, EMD has pronounced spikes of near-perfect reconstruction when the sampling frequency is an even multiple of the tone's frequency.

Here, we perform this analysis for the proposed VMD model. The results for different convergence tolerance levels ϵ are shown in Fig. 3. It can be clearly seen that the relative reconstruction error is largely independent of the harmonic's frequency. Moreover, the relative error is nicely controlled by the tolerance level ϵ.

B. Tones Separation

The next slightly more complicated challenge is the separation of two different superimposed tones [2]. Here, the input signal is composed of two different, pure harmonics:

$$f_{\nu_1,\nu_2}(t) = a_1 \cos(2\pi\nu_1 t) + a_2 \cos(2\pi\nu_2 t), \qquad (31)$$

with $\nu_2 < \nu_1 < f_s/2$, and $a_{1,2}$ two possibly different amplitudes. As a function of the amplitude ratio $\rho = a_1/a_2$, EMD exhibits different, important regions of confusion, where the two signals are too close in frequency to be separated correctly, as reported in [2] and illustrated in Fig. 4.

Again, we apply the same analysis to the proposed VMD model. The results for varying amplitude ratios $\rho \in \{1:4, 1:1, 4:1\}$ are shown in Fig. 4 along with the corresponding EMD error measures. As can be clearly seen, the proposed VMD achieves good tones separation over the whole domain except at the Nyquist frequency. In particular, the decomposition quality is not significantly worse for close harmonics.

C. Noise Robustness

To illustrate the VMD robustness with respect to noise in the input signal, we test using the following tri-harmonic signal,
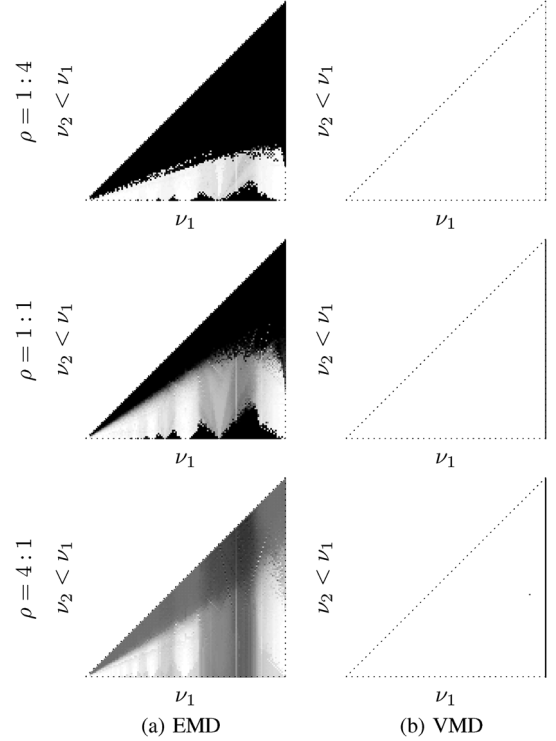

Fig. 4. Tones separation. In a superposition of two tones of frequencies $\nu_2 < \nu_1 < f_s/2$ and amplitudes of different ratio ρ, the mode decompositions between EMD and VMD vary significantly. The plot indicates relative error, with values between 0 (white) and 0.5 (black). (a) EMD has important areas of confusion (dark), where the tones cannot be separated correctly [2]. (b) In contrast, VMD achieves good tones separation almost everywhere but for ν_1 too close to the Nyquist frequency.

affected by noise:

$$f_n(t) = \cos(4\pi t) + \frac{1}{4}\cos(48\pi t) + \frac{1}{16}\cos(576\pi t) + \eta, \quad (32)$$

where $\eta \sim \mathcal{N}(0,\sigma)$ represents the Gaussian additive noise, and σ controls the noise level (standard deviation). Here we pick $\sigma = 0.1$, which is quite important with respect to the amplitude of the highest and weakest harmonic. We perform variational modes decomposition into three modes, without Lagrangian multipliers in order to remove the noise. The signal, and the three components estimated using VMD are shown in Fig. 5. The strong, lowest frequency signal is recovered almost flawlessly. The medium-strength medium-frequency signal is still detected at acceptable quality. The weak, high-frequency signal, however, is difficult. The VMD algorithm correctly tunes the third center-frequency on this harmonic, but the recovered mode is highly affected by the noise. Here, decreasing the bandwidth by increasing α comes at the risk of not properly capturing the correct center frequency, while too low an α includes more noise in the estimated mode. The mode could, however, be cleaned further in post-processing. For reference, we note that the estimated VMD center frequencies are off by 0.27%, 1.11% and 0.18% only.

We provide a comparison with EMD[3] based on exactly the same signal in Fig. 5. The EMD produces 7 estimated modes. The first two modes contain the highest-frequency harmonic,

[3]Implementation by Gabriel Rilling, available at http://perso.ens-lyon.fr/patrick.flandrin/emd.html.

(a) $f_n(t)$

(b) VMD $u_k(t)$

(c) $|\hat{f}_n|(\omega)$

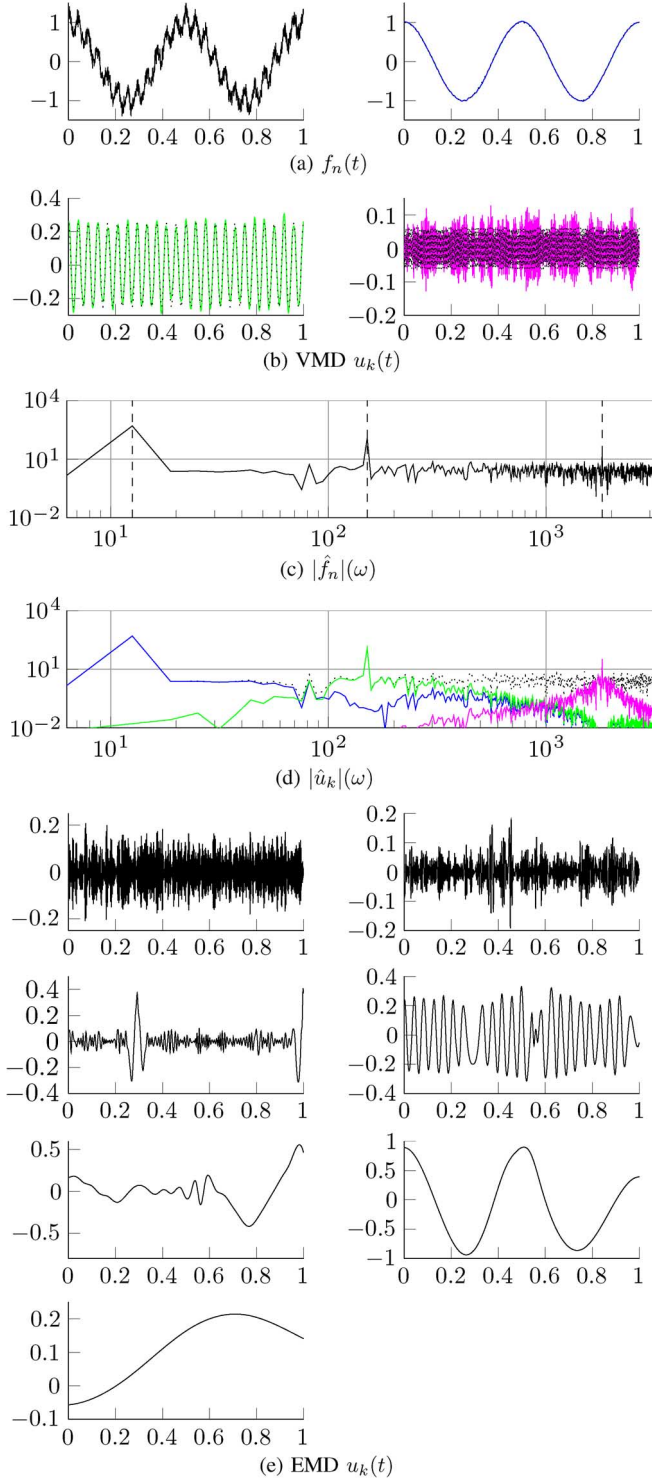(d) $|\hat{u}_k|(\omega)$

(e) EMD $u_k(t)$

Fig. 5. Decomposition of noisy tri-harmonic. (a) The noisy input signal. (b) The three modes extracted by denoising VMD (inactive Lagrangian multiplier), and the theoretical mode (dotted). (c) The spectrum of the input signal (expected mode-frequencies as vertical dashed lines), and (d) its distribution over the three modes. (e) The 7 components extracted by EMD. None of the modes corresponds to a pure harmonic.

and important amounts of noise. The forth mode comes closest to the middle harmonic, however important features have been attributed to the third and fifth mode. The sixth mode picks up most of the low frequency harmonic, but is severely distorted. In addition, we have also run the supposedly noise robust extension of EMD on the same data: Ensemble Empirical Mode
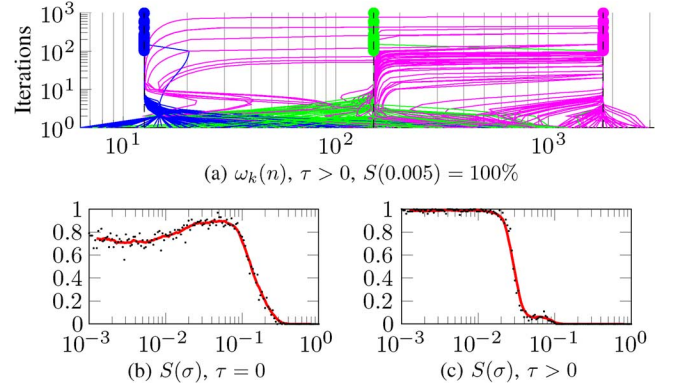

(a) $\omega_k(n)$, $\tau > 0$, $S(0.005) = 100\%$

(b) $S(\sigma)$, $\tau = 0$

(c) $S(\sigma)$, $\tau > 0$

Fig. 6. Convergence and sensitivity to initialization, tested on the noisy tri-harmonic (32). (a) At low noise level, e.g. $\sigma = 0.005$, the Lagrangian multipliers can help achieving 100% success rate despite fully random initialization of center frequencies. (b) Success rate S at higher noise levels σ, without Lagrangian multipliers, and (c) with Lagrangian multipliers. At low noise levels, the Lagrangian multipliers boost the success-rate for random ω_k-initialization to 100%, but with more important noise in the data they become an obstacle.

Decomposition [37]. However, we have not been able to achieve significantly better results than the ones produced by traditional EMD.

D. Initialization and Convergence

Although we cannot provide a detailed convergence analysis in the scope of the present paper, we do wish to comment on some convergence properties and sensitivity to initial conditions. We propose to illustrate the algorithm success for varying random initializations of the center frequencies, the rest of the variables being essentially updated from there.

Indeed, the proposed algorithm is not guaranteed to converge to a global minimum. Therefore, the result does depend on the initialization, and in particular the success rate depends on the noise level. For sufficiently low noise levels, the Lagrangian multiplier can be used to enforce exact reconstruction of the input signal. Therefore, even with unfortunate initialization leading to "duplicate and forgotten modes", the forgotten modes will be picked up eventually. In Fig. 6(a) we show the 100 trajectories of randomly initialized center frequencies for the noisy triharmonic (32), at low noise level $\sigma = 0.005$, and with Lagrangian multipliers active. In this setting, we were 100% successful. The success rate for bigger σ is shown in Fig. 6(c), where one clearly sees the impact of Lagrangian multipliers: Their presence ensures optimal convergence at low noise level, but becomes a strict impediment if noise becomes more important.

In the presence of stronger noise, the Lagrangian multipliers are not useful anymore, since we wish to eliminate the noise from the estimated modes. Here, convergence is more sensitive to noise, and the success rate for the noisy triharmonic (32) drops. A detailed curve of the success rate as a function of the noise level σ is shown in Fig. 6(b). Interestingly, some amount of noise is beneficial with regards to finding the correct center frequencies. Like the non-zero temperature in simulated annealing [38], [39], some noise in the data flattens the spectra and helps the algorithm evolve out of wrong local minima. This leads to maximum success rate of about 90–95% between $\sigma =$
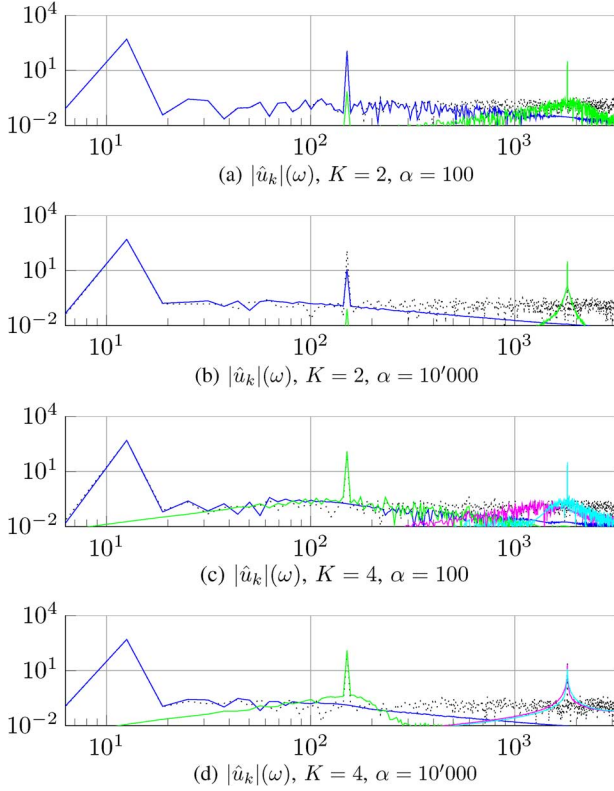
Fig. 7. Sensitivity to the number of modes K. (a), (b) Too few modes lead to undersegmentation of the data. Some components are contained in other modes (low α) or discarded as "noise" (high α and no λ). (c), (d) Too many modes either capture extra noise (α small), or lead to mode duplication (α big). All these cases are easily detected in post-processing.

0.02 and 0.08. Above, the noise starts masking the weakest harmonic and the success rate falls off. The successful trajectories are typically characterized by fast convergence, compared to the failing runs. Also, at $\sigma = 0.1$ for example, all initializations within $14.39 \leq \omega_2 \leq 1050$, and within $743 \leq \omega_3 \leq 2556$ were successful, which means that in this difficult example even the weakest component need only be initialized with an error less than 40% for successful segmentation. This does not seem very strict for a practical application where some prior knowledge about the expected oscillations is available.

E. Over- and Undersegmentation, Uniqueness

A classical shortcoming of many segmentation algorithms is the need to tell in advance into how many clusters (or modes, in the present case), data are to be binned. This is no different with the proposed VMD algorithm. In order to study the effects of over- and underbinning the given data, we evaluate here the outcome of VMD using too few or too many modes, K.

For this study, we use a triharmonic as given in (32), however at small noise level $\sigma = 0.005$. We run VMD both with $K = 2$ (too few modes) and $K = 4$ (too many modes). The resulting decomposition depends on the tightness of the band-limits imposed by the parameter α. Indeed, as shown in Fig. 7, the results are as follows:

When underbinning, one of the modes is either shared by neighboring modes (α small), or mostly discarded (α big and no Lagrangian multipliers). This situation can be identified post-hoc by checking the spectral overlap or orthogonality
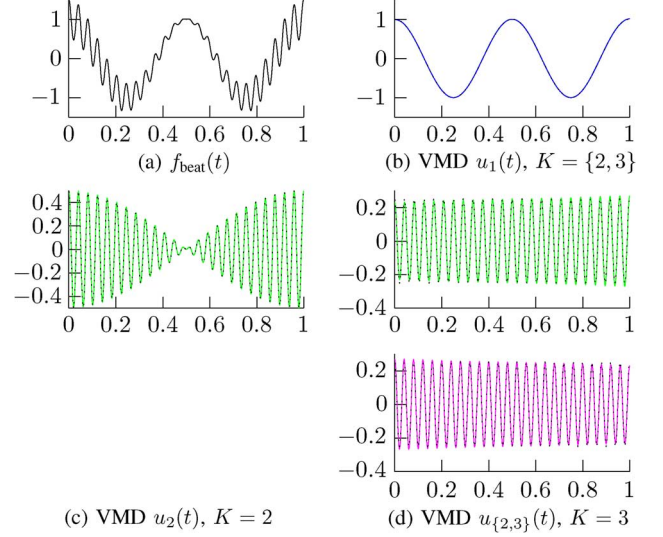

Fig. 8. Decomposition of harmonic beat. (a) The composite signal, with two close harmonics interfering according to (33). (b) The low-frequency harmonic $u_1(t)$ consistently identified for both $K = \{2, 3\}$. (c) The amplitude modulated single mode $u_2(t)$, extracted with $K = 2$. (d) The two constituent single harmonics $u_2(t)$ and $u_3(t)$ found with $K = 3$. The trade-off here is mode bandwidth against number of modes. (a) $f_{\text{beat}}(t)$; (b) VMD $u_1(t)$, $K = \{2, 3\}$; (c) VMD $u_2(t)$, $K = 2$; (d) VMD $u_{\{2,3\}}(t)$, $K = 3$.

between modes to identify portions of the signal shared by several modes, or by looking at the residuals not accounted for by any of the modes ("noise"). Indeed, strongly structured noise would immediately suggest the presence of an extra component not currently accounted for.

On the other hand, when overbinning, the outcome looks more like this: For small α, one or several extra modes will largely consist of noise, and thus have very low structure and broad spectral density. For α big, however, important parts of the signal/spectrum are shared by two or more different modes, and their center frequencies coincide (mode duplication). Again, both situations are easily detected in post-processing, but doing so is beyond the scope of the present manuscript.

The decomposition of a signal in multiple AM-FM signals is not unique. For example, the "beat" effect of two close harmonics is well-known in acoustics. Two harmonics of slightly different pitch $f_1 \approx f_2$ interfere in a way that is perceived as amplitude modulation of a middle harmonic, instead of two individual harmonics, as described by the following trigonometric identity:

$$\cos(2\pi f_1 t) + \cos(2\pi f_2 t) = 2\cos(\pi(f_1 + f_2)t)\cos(\pi(f_1 - f_2)t). \tag{33}$$

The RHS takes the form of an AM-FM signal and is as much an admissible mode function, as are the two individual harmonics. Depending on the number K of modes to be detected, the noise level and imposed bandwidth limits α, VMD can be guided to identify such a signal either as two individual harmonics, or as a single AM-FM mode, shown in Fig. 8. In contrast, EMD will always identify this situation as a single AM-modulated signal (see also Section IV-B on tones separation, above).

F. Non-Stationary Multimode Signals

Now we look at slightly more complex signals to be decomposed. In particular, we consider the same test signals that were
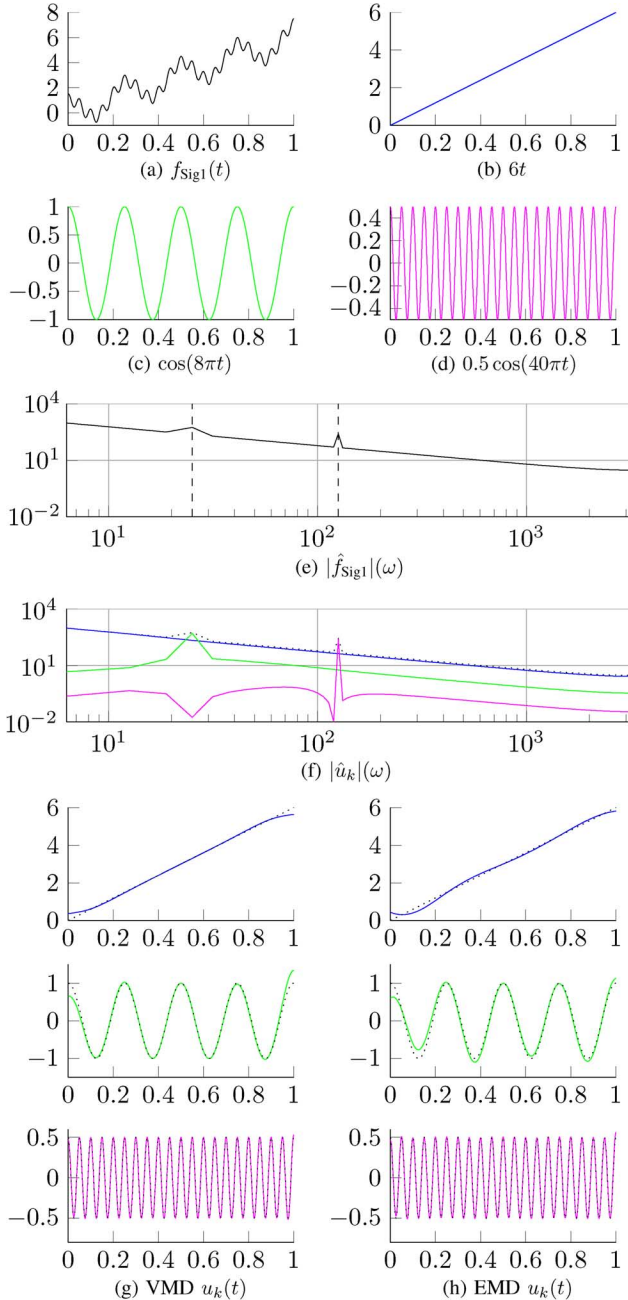
Fig. 9. VMD decomposition of f_{Sig1}. (a) $f_{\text{Sig1}}(t)$, (b)–(d) its constituent modes. (e) The signal's spectrum. (f) VMD's spectral decomposition. (g) VMD reconstructed modes (h) EMD reconstructed modes.

previously suggested in [18] and also used in [14], with the purpose of increased comparability.

1) Example 1: The first signal is a composition of three simple components, namely a general linear trend and two different harmonics:

$$f_{\text{Sig1}}(t) = 6t + \cos(8\pi t) + 0.5\cos(40\pi t). \qquad (34)$$

The signal, its three constituent modes, and the composite Fourier spectrum are shown in Fig. 9. The main challenge of this signal is the linear growth term, whose higher order harmonics spread over the whole spectrum.

The recovered VMD modes constitute a nice partition of the input spectrum, with each mode being clearly dominant around

its respective center frequency. The three modes in time domain show nice separation into three distinct signals of characteristic oscillations. Compared to the EMD results, the proposed VMD method performs clearly better, with less spurious oscillations in the trend and mid-frequency signal.

2) Example 2: The second example uses a quadratic trend, a chirp signal, and a third mode with sharp transition between two constant frequencies:[4]

$$f_{\text{Sig2}}(t) = 6t^2 + \cos(10\pi t + 10\pi t^2) + \begin{cases} \cos(60\pi t) & t \le 0.5 \\ \cos(80\pi t - 10\pi) & t > 0.5 \end{cases}. \qquad (35)$$

The signal, its three constituent modes, and the composite Fourier spectrum are shown in Fig. 10. For $t \in [0, 1]$ the chirp's instantaneous frequency varies linearly between 10π an 30π. Consequently, the theoretical center frequency of the mode is located at 20π. The piecewise-constant bi-harmonic has spectral peaks expected at 60π and 80π.

Again, with VMD the estimated center frequencies ω_k converge to the expected frequencies precisely. Here, we chose to decompose into four modes, thus assigning each half of the piecewise-constant frequency signal to a separate mode. The spectral partitioning can be nicely appreciated in the spectral plot of the different modes. Here, EMD does a better job recovering the quadratic trend, and, correspondingly, the first oscillation. However, EMD is unable to separate the two pieces of the piecewise constant frequency signal.

3) Example 3: The third synthetic signal has intrawave frequency modulation:

$$f_{\text{Sig3}}(t) = \frac{1}{1.2 + \cos(2\pi t)} + \frac{\cos(32\pi t + 0.2\cos(64\pi t))}{1.5 + \sin(2\pi t)}. \qquad (36)$$

The signal, its three constituent modes, and the composite Fourier spectrum are shown in Fig. 11. While the first, bell-shaped component has mostly low-pass content, the second mode's main peak is clearly identified at 32π. However, due to the non-linear intrawave frequency modulation, an important amount of higher-order harmonics are also observed. This second component obviously violates the narrow-band assumption, and one would naturally expect some difficulties recovering this mode using VMD.

The corresponding VMD results are illustrated in Fig. 11. The non-zero ω_2 quickly converges to the correct main frequency 32π. The higher order harmonics are not uniquely attributed to the second mode, however, but shared between both modes. Consequently, the intrawave frequency modulation is shared by both modes, creating some ripples in the otherwise low-frequency mode.

4) Example 4: The forth signal is a superposition of two sawtooth-signals of different period and amplitude, as illustrated in Fig. 12. We chose to test this signal since its natural modes are admitted by the original definition of modes by Huang [1], but conflict with the newer IMF definition which serves as starting point for the proposed method. Indeed, the sawtooth signal has

[4]Here, we changed the phase shift in the third component, with piecewise-constant frequency, from 15π to 10π, in order to have a continuous signal.
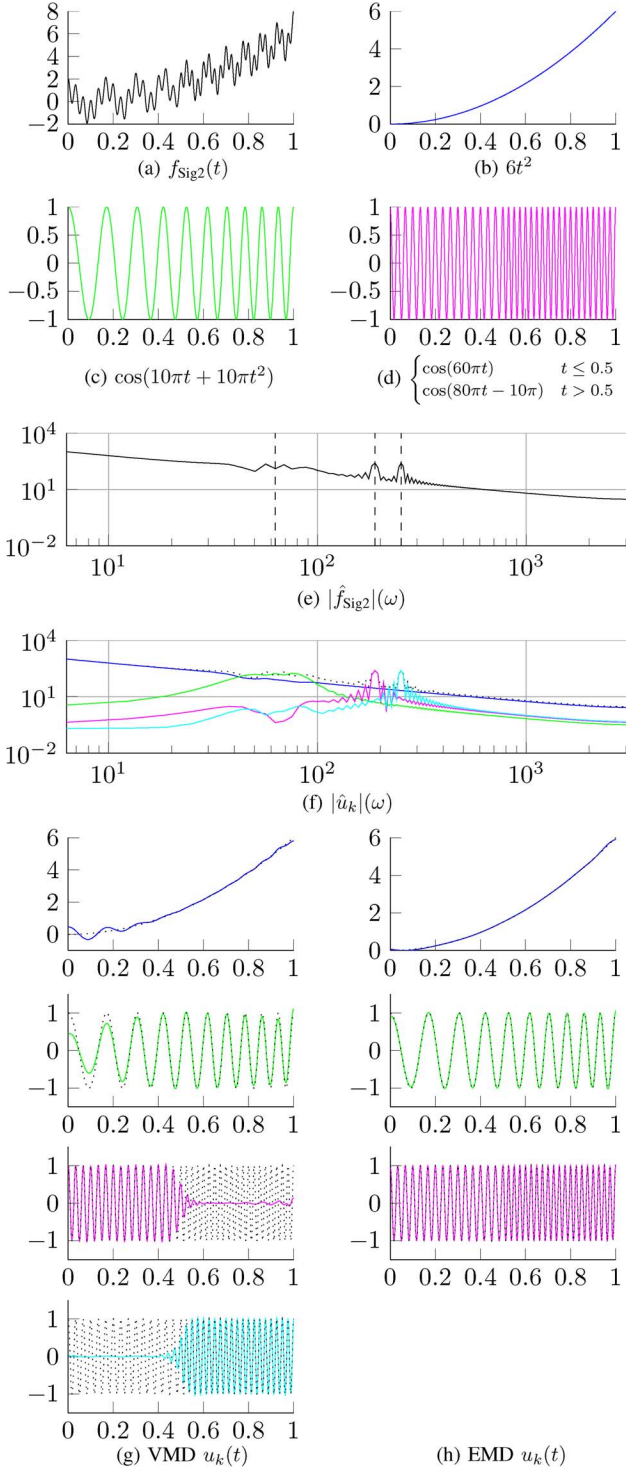
Fig. 10. Results of VMD and EMD on f_{Sig2}. (a) f_{Sig2}, (b)–(d) its constituent modes. (e) The signal's spectrum. (f) VMD's spectral decomposition. (g) VMD reconstructed modes. (h) EMD reconstructed modes.

Fig. 11. Results of VMD on f_{Sig3}. (a) f_{Sig3}, (b), (c) its constituent modes. (d) The signal's spectrum. (e) The corresponding spectrum decomposition. (f) VMD reconstructed modes. (g) EMD reconstructed modes.

important higher order harmonics, that spread over the full spectrum, and even create aliasing, which is in clear violation of the limited band-width assumption of VMD modes.

The results of the decomposition are quite surprising, though. Indeed, the proposed VMD algorithm captures the relevant center frequencies quite precisely, and the resulting signal separation is relatively good. Only a few spikes spill over
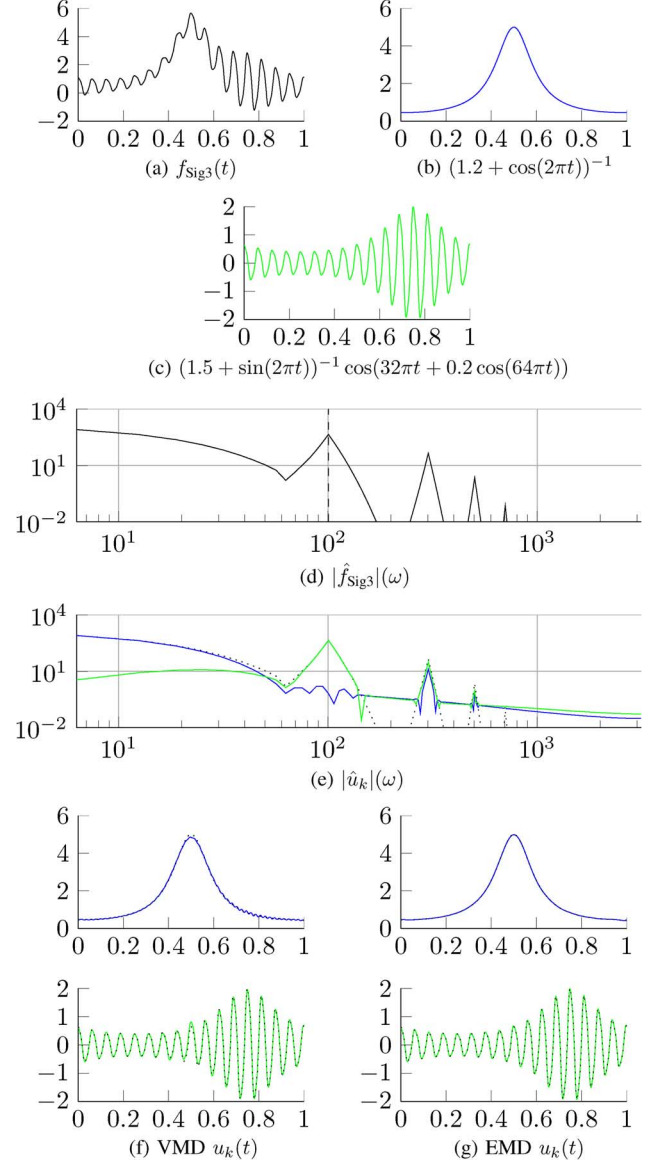
from the somewhat smoothed low-frequency sawtooth over into the higher-frequency component. In contrast, the EMD decomposition fails to properly extract the highest frequency oscillations. As a result, the residual after the first sifting is still heavily contaminated by the higher-frequency sawtooth.

5) Example 5: The fifth example is a real signal from an electrocardiogram (ECG), data shared by [14]. These data present numerous components, as seen in Fig. 13. Beyond the expected spikes-train driven by the rhythm of the heartbeat, one can clearly see an oscillating low-frequency pattern. At the other end of the spectrum, there is distinct high-frequency noise at a single high-pitch harmonic, most likely the electric power-line frequency. The distinct spikes of the ECG signal create important higher-order harmonics.

The spectrum and the results of VMD are depicted in Fig. 13. We chose a high-number of 10 modes to be detected, to accommodate the numerous higher-order harmonics of the spikes. The
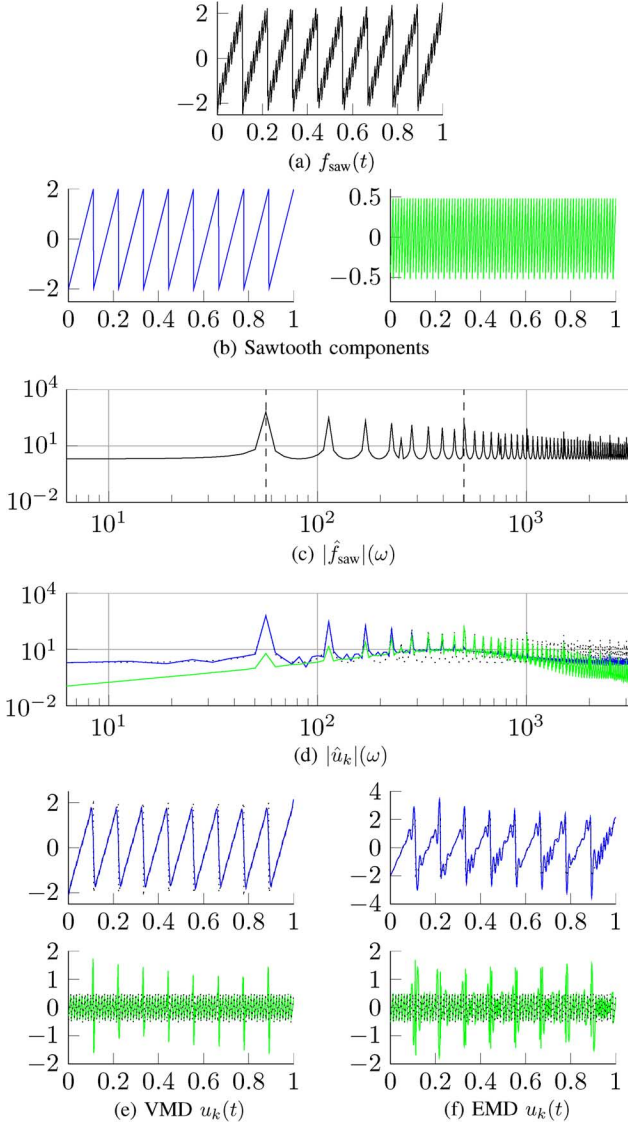
Fig. 12. Results of VMD and EMD on f_{saw}. (a) f_{saw}, (b) its constituent modes. (c) The signal's spectrum. (d) The corresponding spectrum decomposition. (e) VMD reconstructed modes. (f) EMD reconstructed modes.

Fig. 13. Results of ECG decomposition. (a), (b) ECG and detail. (c) The signal's spectrum. (d) Reconstructed modes. (e), (f) Cleaned ECG and detail.

respective center frequencies nicely converge to these spectral peaks. The first, low-frequency mode captures the low-frequency oscillation of the baseline. The highest frequency mode contains the most noise. The first actual ECG specific mode oscillates precisely at the frequency of the heartbeat. The higher ECG modes then contain the higher-order wave-packages around the highly non-sinusoidal spikes. A "clean" ECG signal can be reconstructed by summing all but the first and last VMD modes, thus discarding the low-frequency baseline oscillation and most of the high-frequency noise.

V. CONCLUSIONS AND OUTLOOK

In this paper, we have presented a novel variational method for decomposing a signal into an ensemble of band-limited intrinsic mode functions, that we call Variational Mode Decomposition, (VMD). In contrast to existing decomposition models, like the empirical mode decomposition (EMD), we refrain from modeling the individual modes as signals with explicit IMFs.
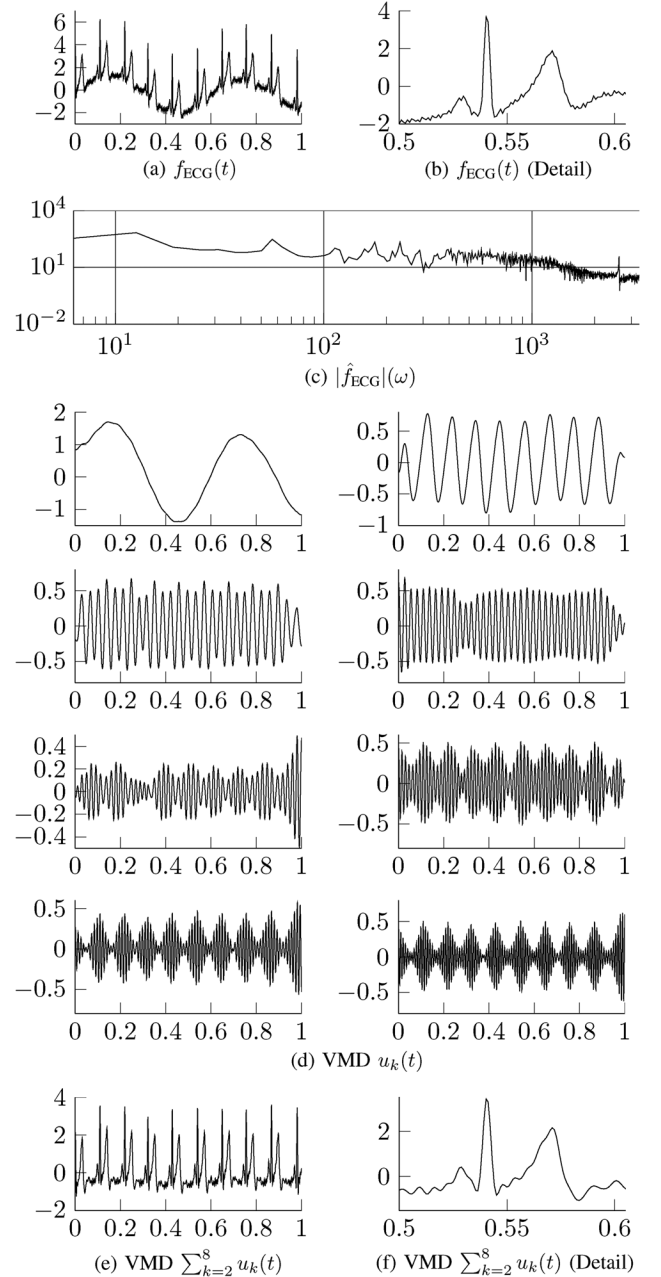
Instead, we replace the most recent definition of IMFs, namely their characteristic description as AM-FM signals, by the corresponding narrow-band property. Indeed, we provide a formula that relates the parameters of the explicit AM-FM descriptors to the estimated signal bandwidth.

Our decomposition model solves the inverse problem as follows: decompose a signal into a given number of modes, either exactly or in a least squares sense, such that each individual mode has limited bandwidth. We assess the mode's bandwidth as the squared H^1 norm of its Hilbert complemented analytic signal with only positive frequencies, shifted to baseband by mixing with a complex exponential of the current center frequency estimate. The variational problem is solved very efficiently in a classical ADMM approach: The modes are updated

by simple Wiener filtering, directly in Fourier domain with a filter tuned to the current center frequency, then the center frequencies are updated as the center of gravity of the mode's power spectrum, and finally the Lagrangian multiplier enforcing exact signal reconstruction is updated as dual ascent.

Since the Fourier transform corresponds to an expansion in an orthonormal basis, two signals having non-overlapping support in their Fourier spectra are inherently orthogonal. The decomposed mode functions obtained through the proposed VMD algorithm have largely disjoint spectral support and are therefore automatically quasi-orthogonal. This corresponds well to the quasi-orthogonality property mentioned with EMD, e.g. [17].

In our experiments, we show that the proposed VMD scheme clearly outperforms EMD with regards to tone detection, tone separation, and noise robustness. Further, we apply our model to more complicated signals for comparison with other state-of-the-art methods, and can show successful decomposition.

The core assumption of VMD is the limited bandwidth of the individual modes. The most important resulting limitation of the proposed VMD is with boundary effects, and sudden signal onset in general. This is strongly related to the use of an L^2-based smoothness term, that overly penalizes jumps at the domain borders and within; conversely, this is also reflected by implicit periodicity assumptions when optimizing in Fourier domain, and by the narrow-band violation caused by discontinuous envelopes in such AM-FM signals. The proposed VMD model does not explicitly deal with a global trend in the signal. However, in our code we do include an option to fix the center frequency of one mode at $\omega_1 = 0$, which can address the prior knowledge about the existence of a very low frequency component in the signal. Due to the strongly non-periodic nature of this trend and despite the mirror extension at the boundaries, a strong trend will spread its harmonics over the whole signal spectrum, and in some cases it might be crucial to eliminate strong trends preliminarily, using classical trend removal approaches.

VMD does not work "out of the box" with non-stationary signals, like long-term EEG records, for which the spectral bands of modes can change more drastically over time, and will globally overlap. Here, the direct solution is to break down the decomposition on shorter chunks, on which the signals are sufficiently stationary. This is classically done so in short-term Fourier analysis. There also, the chunk borders are dealt with by smooth windowing as opposed to mirror extension, see e.g. [40], [41]. The window is simply applied to the input signal chunk f prior to performing the VMD algorithm. In a sliding window short-time analysis of a larger time series signal, the modes can be stitched together by simple weighted addition, a synthesis method called weighted overlap-add (OLA) [41], [42]. For greater coherence of modes across the sliding windows, temporal filtering might then become useful [43].

Also, our method requires the number of modes to be predefined. This is a vice we share with many successful clustering and segmentation algorithms, like k-means [44], [45]. The empirical wavelet transform suffers from the same drawback [14]. In practical applications, prior information about the expected number of modes should be available most of the time, at least up to some precision. Beyond, we have found that both overbinning and underbinning have predictable impact on the nature of detected modes, and thus criteria for automatic determination of K could be devised.

Current work addresses these shortcomings, and we are also working on suitable extensions to signals on domains of dimension greater than one.

A MATLAB implementation of the proposed algorithm is available at http://www.math.ucla.edu/~zosso/code.html.

REFERENCES

[1] N. E. Huang, Z. Shen, S. R. Long, M. C. Wu, H. H. Shih, Q. Zheng, N.-C. Yen, C. C. Tung, and H. H. Liu, "The empirical mode decomposition and the Hilbert spectrum for nonlinear and non-stationary time series analysis," *Proc. Royal Soc. A: Math., Phys. Eng. Sci.*, vol. 454, no. 1971, pp. 903–995, Mar. 1998.

[2] G. Rilling, P. Flandrin, and P. Gonçalvès, "On empirical mode decomposition and its algorithms," in *Proc. IEEE-EURASIP Workshop Nonlinear Signal Image Process. (NSIP)*, 2003, vol. 3, pp. 8–11.

[3] R. C. Sharpley and V. Vatchev, "Analysis of the intrinsic mode functions," *Construct. Approx.* vol. 24, no. 1, pp. 17–47, Aug. 2005.

[4] G. Rilling and P. Flandrin, "One or two frequencies? The empirical mode decomposition answers," *IEEE Trans. Signal Process.*, vol. 56, no. 1, pp. 85–95, Jan. 2008.

[5] G. Rilling and P. Flandrin, "Sampling effects on the empirical mode decomposition," *Adv. Adapt. Data Anal.*, vol. 01, no. 01, pp. 43–59, Jan. 2009.

[6] P. Flandrin, P. Gonçalvès, and G. Rilling, "EMD equivalent filter banks, from interpretation to applications," in *Hilbert-Huang Transform Its Appl.*, 2005, pp. 57–74.

[7] N. Klügel, "Practical empirical mode decomposition for audio synthesis," in *Proc. Int. Conf. Digital Audio Effects (DAFx-12)*, 2012, no. 2, pp. 15–18.

[8] B. Barnhart and W. Eichinger, "Empirical mode decomposition applied to solar irradiance, global temperature, sunspot number, and CO2 concentration data," *J. Atmospher. Solar-Terrestrial Phys.*, vol. 73, no. 13, pp. 1771–1779, Aug. 2011.

[9] S. Assous, A. Humeau, and J.-P. L'huillier, "Empirical mode decomposition applied to laser Doppler flowmetry signals: Diagnosis approach," in *Proc. IEEE Eng. Med. Biol. Conf. (EMBC)*, Jan. 2005, vol. 2, pp. 1232–1235.

[10] A. O. Andrade, S. Nasuto, P. Kyberd, C. M. Sweeney-Reed, and F. Van Kanijn, "EMG signal filtering based on empirical mode decomposition," *Biomed. Signal Process. Control*, vol. 1, no. 1, pp. 44–55, Jan. 2006.

[11] S. Liu, Q. He, R. X. Gao, and P. Freedson, "Empirical mode decomposition applied to tissue artifact removal from respiratory signal," in *Proc. IEEE Eng. Med. Biol. Conf. (EMBC)*, Jan. 2008, pp. 3624–3627.

[12] I. Mostafanezhad, O. Boric-Lubecke, V. Lubecke, and D. P. Mandic, "Application of empirical mode decomposition in removing fidgeting interference in Doppler radar life signs monitoring devices," in *Proc. IEEE Eng. Med. Biol. Conf. (EMBC)*, Jan. 2009, pp. 340–343.

[13] I. Daubechies, J. Lu, and H.-T. Wu, "Synchrosqueezed wavelet transforms: An empirical mode decomposition-like tool," *Appl. Computat. Harmon. Anal.*, vol. 30, no. 2, pp. 243–261, Mar. 2011.

[14] J. Gilles, "Empirical wavelet transform," *IEEE Trans. Signal Process.*, vol. 61, no. 16, pp. 3999–4010, Aug. 2013.

[15] J. Carson, "Notes on the theory of modulation," *Proc. IRE*, vol. 10, no. 1, pp. 57–64, Feb. 1922.

[16] S. Meignen and V. Perrier, "A new formulation for empirical mode decomposition based on constrained optimization," *IEEE Signal Process. Lett.* vol. 14, no. 12, pp. 932–935, Dec. 2007.

[17] N. Pustelnik, P. Borgnat, and P. Flandrin, "A multicomponent proximal algorithm for empirical mode decomposition," in *Proc. IEEE 20th Eur. Signal Process. Conf. (EUSIPCO)*, 2012, pp. 1880–1884.

[18] T. Y. Hou and Z. Shi, "Adaptive data analysis via sparse time-frequency representation," *Adv. Adapt. Data Anal.*, vol. 03, no. 1 & 2, pp. 1–28, Apr. 2011.

[19] M. Feldman, "Time-varying vibration decomposition and analysis based on the Hilbert transform," *J. Sound Vibrat.*, vol. 295, no. 3–5, pp. 518–530, Aug. 2006.

[20] H.-T. Wu, P. Flandrin, and I. Daubechies, "One or two frequencies? The synchrosqueezing answers," *Adv. Adapt. Data Anal.*, vol. 03, no. 01–02, pp. 29–39, Apr. 2011.

[21] I. W. Selesnick, "Resonance-based signal decomposition: A new sparsity-enabled signal analysis method," *Signal Process.*, vol. 91, no. 12, pp. 2793–2809, Dec. 2011.

[22] J. Hadamard, "Sur les problèmes aux dérivées partielles et leur signification physique," *Princeton Univ. Bull.*, vol. 13, pp. 49–52, 1902.

[23] M. Bertero, T. A. Poggio, and V. Torre, "Ill-posed problems in early vision," *Proc. IEEE*, vol. 76, no. 8, pp. 869–889, 1988.

[24] A. N. Tichonov, "Solution of incorrectly formulated problems and the regularization method," *Soviet Math.*, vol. 4, pp. 1035–1038, 1963.

[25] V. A. Morozov, "Linear and nonlinear ill-posed problems," *J. Math. Sci.*, vol. II, no. 6, pp. 706–736, 1975.

[26] N. Wiener, *Extrapolation, Interpolation, and Smoothing of Stationary Time Series With Engineering Applications*. Cambridge, MA, USA: Technology Press of Mass. Inst. of Technol., 1949.

[27] R. C. Gonzalez and R. E. Woods, *Digital Image Processing*. Reading, MA, USA: Addison-Wesley, 1992.

[28] M. Unser, D. Sage, and D. Van De Ville, "Multiresolution monogenic signal analysis using the Riesz–Laplace wavelet transform," *IEEE Trans. Image Process.*, vol. 18, no. 11, pp. 2402–2418, 2009.

[29] S. L. Hahn, *Hilbert Transforms in Signal Processing*. Norwood, MA, USA: Artech House, 1996.

[30] D. Gabor, "Theory of communication," *J. Inst. Elect. Eng.—Part III: Radio Commun. Eng.*, vol. 93, no. 26, pp. 429–457, 1946.

[31] E. Bedrosian, "A product theorem for Hilbert transforms," *Proc. IEEE*, vol. 51, no. 5, pp. 868–869, 1963.

[32] D. P. Bertsekas, "Multiplier methods: A survey," *Automatica*, vol. 12, no. 2, pp. 133–145, 1976.

[33] J. Nocedal and S. J. Wright, *Numerical Optimization*, 2nd ed. Berlin, Germany: Springer, 2006.

[34] M. R. Hestenes, "Multiplier and gradient methods," *J. Optimiz. Theory Appl.*, vol. 4, no. 5, pp. 303–320, 1969.

[35] R. T. Rockafellar, "A dual approach to solving nonlinear programming problems by unconstrained optimization," *Math. Program.*, vol. 5, no. 1, pp. 354–373, Dec. 1973.

[36] D.P. Bertsekas, "Constrained optimization and Lagrange Multiplier methods," in *Computer Science and Applied Mathematics*. Boston, MA, USA: Academic, 1982, vol. 1.

[37] Z. Wu and N. E. Huang, "Ensemble empirical mode decomposition: A noise-assisted data analysis method," *Adv. Adapt. Data Anal.*, vol. 01, no. 01, pp. 1–41, Jan. 2009.

[38] S. Kirkpatrick, C. D. Gelatt, and M. P. Vecchi, "Optimization by simulated annealing," *Science*, vol. 220, no. 4598, pp. 671–680, May 1983.

[39] M. W. Trosset, "What is simulated annealing?," *Optimiz. Eng.*, vol. 2, pp. 201–213, 2001.

[40] J. Allen, "Short term spectral analysis, synthesis, and modification by discrete Fourier transform," *IEEE Trans. Acoust., Speech, Signal Process.*, vol. 25, no. 3, pp. 235–238, Jun. 1977.

[41] J. Allen and L. Rabiner, "A unified approach to short-time Fourier analysis and synthesis," *Proc. IEEE*, vol. 65, no. 11, pp. 1558–1564, 1977.

[42] R. Crochiere, "A weighted overlap-add method of short-time Fourier analysis/synthesis," *IEEE Trans. Acoust., Speech, Signal Process.*, vol. 28, no. 1, pp. 99–102, Feb. 1980.

[43] R. Bitmead and P. Parker, "A Kalman filtering approach to short-time Fourier analysis," *IEEE Trans. Acoust., Speech, Signal Process.*, vol. 34, no. 6, pp. 1493–1501, Dec. 1986.

[44] H. Bock, "Clustering methods: A history of k-means algorithms," *History*, pp. 161–172, 1979.

[45] A. K. Jain, "Data clustering: 50 years beyond K-means," *Pattern Recogn. Lett.*, vol. 31, pp. 651–666, 2010.

Konstantin Dragomiretskiy received the B.S. (Hons.) degree in mathematics and the B.A. degree in economics from the University of California, San Diego, in 2010.

He was an Intern Researcher at Sun Microsystems, Menlo Park, CA, in 2006, and an Undergraduate Researcher at California State University, Chico, in 2008. He is currently a Research Assistant at the Department of Mathematics at the University of California, Los Angeles, working towards the Ph.D. degree with Prof. Andrea L. Bertozzi. His current research interests include variational and PDE based methods applied to signal and image processing problems.

Dominique Zosso (S'06–M'11) received the M.Sc. degree in electrical and electronics engineering and the Ph.D. degree from École Polytechnique Fédérale de Lausanne (EPFL), Lausanne, Switzerland, in 2006 and 2011, respectively.

He was a Researcher with the Structural Bioinformatics Group at the Swiss Institute of Bioinformatics and Biozentrum, University of Basel, Basel, Switzerland, from 2006 to 2007. He was Research and Teaching Assistant at the Signal Processing Laboratory, EPFL, from 2007 to 2012. He is currently a Postdoctoral fellow and CAM Assistant Adjunct Professor with the Department of Mathematics, University of California, Los Angeles, CA, working with Luminita A. Vese, Andrea L. Bertozzi, and Stanley J. Osher. His research interests include PDE and variational models for inverse problems in computer vision, signal and image processing, and efficient algorithms to solve them.